Chinese Chemical Letters 36 (2025) 110178

Contents lists available at ScienceDirect

Chinese Chemical Letters

journal homepage: www.elsevier.com/locate/cclet

A β-lapachone-loaded iron-polyphenol nanocomplex enhances chemodynamic therapy through cascade amplification of ROS in tumor

Xueying Shi[a,1], Xiaoxuan Zhou[b,1], Bing Xiao[a,c], Hongxia Xu[a], Wei Zhang[a], Hongjie Hu[b], Shiqun Shao[a], Zhuxian Zhou[a], Youqing Shen[a], Xiaodan Xu[a,*], Jianbin Tang[a,*]

[a] Zhejiang Key Laboratory of Smart Biomaterials, ZJU-Hangzhou Global Scientific and Technological Innovation Center, and College of Chemical and Biological Engineering, Zhejiang University, Hangzhou 310027, China
[b] Department of Radiology, Sir Run Run Shaw Hospital (SRRSH) of School of Medicine, Zhejiang University, Hangzhou 310027, China
[c] Zhejiang Province Key Laboratory of Anti-Cancer Drug Research, College of Pharmaceutical Sciences, Zhejiang University, Hangzhou 310058, China

ARTICLE INFO

Article history:
Received 28 April 2024
Revised 21 June 2024
Accepted 25 June 2024
Available online 25 June 2024

Keywords:
Cascade amplification of ROS
Tumor-selectivity
Chemodynamic therapy
Immunogenic cell death
Enhanced cancer therapy

ABSTRACT

Chemodynamic therapy (CDT), using Fenton agents to generate highly cytotoxic ·OH from H_2O_2 has been demonstrated as a powerful anticancer method. However, the insufficient endogenous H_2O_2 in tumor cells greatly limited its therapeutic effect. Herein, we prepared a pH-responsive β-lapachone-loaded iron-polyphenol nanocomplex (LIPN) through a one-pot method. β-Lapachone in LIPN selectively enhanced H_2O_2 concentration in tumor cells, and ferrous ions cascadely generated abundant cytotoxic ·OH. Therefore, LIPN with cascade amplification of reactive oxygen species (ROS) showed high chemodynamic cytotoxicity in tumor cells, efficiently improving the expression of damage-associated molecular patterns (DAMPs), and exerting strong immunogenic cell death (ICD). As a result, LIPN exhibited efficient tumor inhibition ability in 4T1 subcutaneous tumor model *in vivo* with great biocompatibility. Additionally, the infiltration of cytotoxic $CD8^+$ T lymphocytes and inhibition of regulatory $CD4^+$ $FoxP3^+$ T lymphocytes in tumors demonstrated the activation of immunosuppressive tumor microenvironment by LIPN-induced ICD. Therefore, this work provided a new approach to enhance ICD of chemodynamic therapy through selective cascade amplification of ROS in cancer cells.

Despite chemotherapy has been widely applied in tumor therapy [1,2], the adverse side effects and unsatisfactory therapeutic outcomes caused by poor tumor selectivity and immunosuppressive tumor microenvironment limit its further development [3-5]. Immunogenic cell death (ICD), which greatly augments tumor immunogenicity *via* the release of various damage-associated molecular patterns (DAMPs), provides a promising strategy to increase the antitumor immune effect and patient response rates [6-8]. Many chemo-drugs like doxorubicin (DOX) [9], oxaliplatin [10], and shikonin [11] have been proved to induce ICD successfully by elevating cellular reactive oxygen species (ROS) in tumors [12], improving the tumor immunosuppressive microenvironment. However, the ROS generation is still not enough to elicit strong ICD for efficient immunotherapeutic effect.

Chemodynamic therapy (CDT), a new tumor treatment strategy using Fenton or Fenton-like agents to exert toxic hydroxyl radical (·OH) to kill tumor cells, has been recently proposed [13-20]. Several metal ions including copper, iron, and manganese ions, could act as Fenton agents to transform endogenous H_2O_2 to a stronger oxidizing ·OH to induce lethal oxidative damage in the tumor [21-24]. For instance, an intelligent nanoreactor that was capable of triggering Fenton reaction with Cu^{2+} was prepared for enhancing the ICD effect and regulating the tumor immune microenvironment, leading to synergistic chemotherapy or photodynamic therapy (PDT)/immunotherapy [22,25,26]. Mao *et al.* fabricated a nanomedicine through complexation of various polyphenol segments with Fe^{3+} to improve the anticancer capability of Pt(IV) complexes by elevating ·OH [27]. However, the insufficient endogenous H_2O_2 and limited ·OH levels in tumor cells greatly compromised treatment outcome. Thus, selectively amplifying intracellular oxidative stress in tumor to further enhance ICD is highly desired.

β-Lapachone (β-LP) has been proved to generate extensive H_2O_2 under the catalysis of nicotinamide adenine dinucleotide (phosphate) (NAD(P)H): quinone oxidoreductase-1 (NQO1) enzyme overexpressed in tumor cells [28]. In this aspect, our previous research about cascade amplification release micelles showed the

* Corresponding authors.
E-mail addresses: xuxiaodan@zju.edu.cn (X. Xu), jianbin@zju.edu.cn (J. Tang).
[1] These authors contributed equally to this work.

https://doi.org/10.1016/j.cclet.2024.110178
1001-8417/

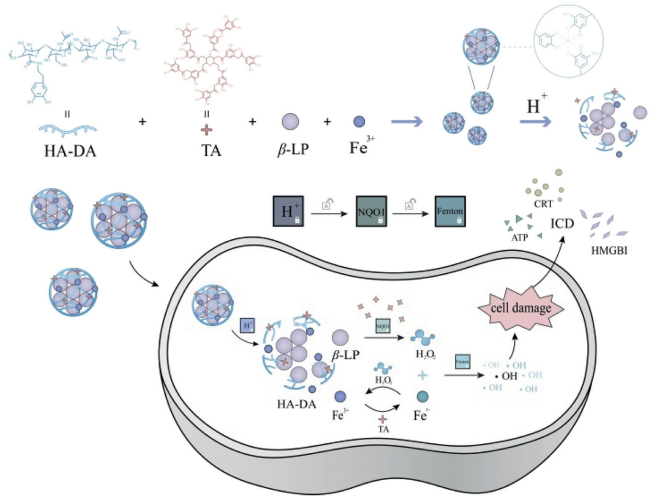

Scheme 1. Schematic illustration of a β-lapachone-loaded iron-polyphenol nanocomplex (LIPN) with cascade amplification of oxidative stress and immunogenic cell death to enhance synergistic chemodynamic and immune cancer therapy.

abundant ROS produced by β-LP could specifically activate the prodrug of DOX in the tumor [29]. Similarly, β-LP was co-delivered with paclitaxel, nitrogen mustard, and camptothecin-based prodrugs to achieve synergistic chemotherapy [30-32]. Therefore, β-LP can be used to selectively amplify H_2O_2 in tumor, which cascadely enhances Fenton reaction in tumor cells to generate toxic $^{\bullet}OH$. As a result, an exaggerated oxidative damage to tumor cells with enhancing ICD effect can be achieved to improve chemotherapy efficacy.

Herein, we constructed a pH-responsive nanocomplex LIPN (β-lapachone-loaded iron-polyphenol nanocomplex) through the coordination of Fe^{3+}, tannic acid (TA), and hyaluronic acid modified with dopamine (HA-DA), and the simultaneous encapsulation of β-LP, which achieving cascade amplification of ROS and efficient anticancer efficacy through inducing the immunogenic cell death (Scheme 1). The formed LIPN could accumulate in the tumor through the enhanced permeability and retention (EPR) effect [3], and disassociate to release β-LP, Fe^{3+}, and TA in the acidic tumor microenvironment. The released β-LP selectively increased the H_2O_2 level under the efficient catalysis of NQO1 enzyme overexpressed in tumor cells. Meanwhile, the coexistence of excessive TA enables gradual conversion of both the disintegrated Fe^{3+} toward Fe^{2+} [33] and enhanced H_2O_2 would react with generated Fe^{2+} to amplify the generation of $^{\bullet}OH$, further increasing intracellular ROS production and achieving cascade self-amplification to enhance the ability of ICD. Importantly, the cascade amplification of ROS will not happen in normal tissues, because they do not overexpress NQO1, which can avoid the side effect from the treatment. Therefore, this work demonstrated a novel strategy to improve the ICD of chemodynamic therapy through selectively cascade amplification of ROS in cancer cells.

To develop an efficient cascade ROS-generating nanoparticle with immunogenic cell death for cancer therapy, LIPN was fabricated by utilizing the strong coordination effect between Fe^{3+} and polyphenols under the protection of HA-DA, whose degree of dopamine substitution was determined by ^1H NMR to be 38% (Fig. S1a in Supporting information). Transmission electron microscopy (TEM) showed that LIPN was spherical nanoparticle. Dynamic light scattering (DLS) indicated that LIPN has a volume-averaged hydrodynamic diameter of 70 nm and zeta potential of −22.7 mV (Figs. 1a and b, Fig. S1b in Supporting information). After extracting β-LP with acetonitrile, the nanoparticles became hollow nanocapsules with *ca.* 20 nm shells (Fig. 1c), which indicated the efficient encapsulation of β-LP. The encapsulation content and efficiency of β-LP tested by high-performance liquid chromatography (HPLC) were 21.0% and 34.2%, respectively. The mass ratio of Fe in the nanoparticles characterized by inductively coupled plasma mass spectrometry (ICP-MS) was determined to be 1.6% which was similar to the energy dispersive spectrometer (EDS) result (1.3%, Fig. S2 in Supporting information). Additionally, as shown in Fig. S3 (Supporting information), the iron that existed in LIPN was found to be ferric ions from the examination of X-ray photoelectron spectroscopy (XPS) showing typical binding energy peaks of 716 eV and 725 eV, which were represented for Fe $2p_{3/2}$ and Fe $2p_{1/2}$, respectively [34]. Moreover, LIPN exhibited promising stability in water, phosphate buffered saline (PBS), saline, and 10% serum during 7 days (Fig. S4 in Supporting information). These results indicated that β-LP formed a nanocrystal core by solvent exchange with the adhesion of polyphenol-Fe^{3+} complex successfully. The pH-responsive release profiles of β-LP from LIPN were measured at pH 7.4, 6.5, 5.0, and 4.0, respectively. As shown in Fig. 1d, more rapid release profiles for β-LP were observed at pH 5.0 and 4.0, with about 60% β-LP released under pH 4.0 in 4 h, while β-LP showed a slow-release profile at pH 7.4. This phenomenon could be explained by a pH-dependent coordinated structural dissociation of TA-Fe nanocomplex [35].

TA could act as a reductant in the iron cycling to supply Fe^{2+} as a Fenton agent continuously [36]. As a reduction-oxidation (REDOX) indicator, *o*-phenanthroline is often used to detect the existence of Fe^{2+} through the formation of an orange complex. Fig. S5 (Supporting information) showed that the appearance of orange solution (Fe^{2+} indicator) validated the deduction process of TA and Fe^{3+}. Specifically, the image showed that pH 4.0 was more suitable for TA to reduce Fe^{3+} compared to pH 7.4. The HA-DA was also tested and showed negligible reducing ability. The resultant

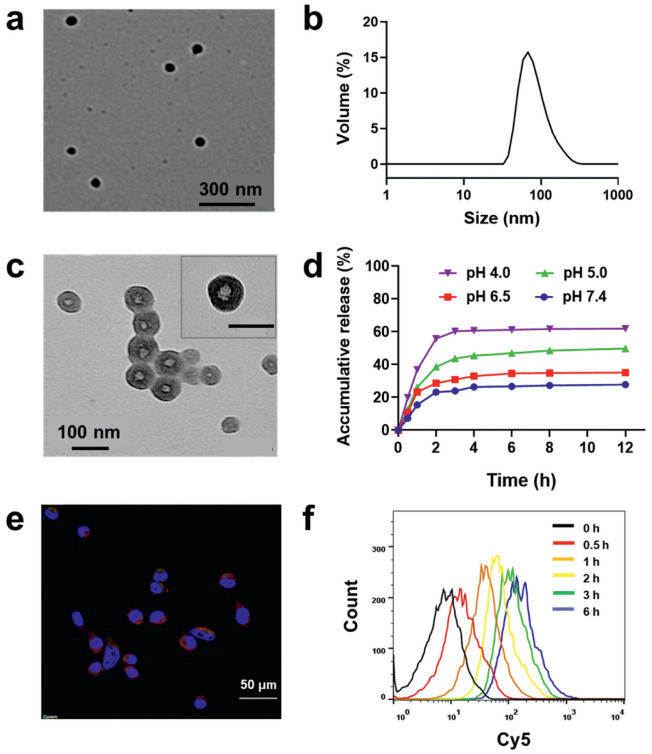

Fig. 1. (a) TEM image and (b) size of LIPN measured by DLS. (c) TEM image of LIPN after etching with acetonitrile. (d) β-LP release profiles of LIPN under different pH conditions. (e) CLSM image of 4T1 cells incubated with Cy5-labeled LIPN for 1 h. (f) Flow cytometry results of the time-dependent uptake of Cy5-labeled LIPN by 4T1 cells. Data are presented as mean ± standard deviation (SD) ($n = 3$).

solution of Fe^{2+} could react with H_2O_2 to induce Fenton reaction and change to colorless at pH 4.0, which proved the consumption of Fe^{2+}. On the contrary, when the colorless solution containing Fe^{2+} and H_2O_2 was further added by TA, it turned orange again, demonstrating the continuous supply of Fe^{2+} by TA. Moreover, the resultant Fe^{2+} could react with H_2O_2 to conduct Fenton reaction. Thus, two commonly used free radical indicators, methylene blue (MB) and 3,3′,5,5′-tetramethylbenzidine (TMB), were applied to detect ·OH generated from LIPN [37]. Considering that ·OH could induce color fading of MB and rendering of TMB when LIPN existed in an acidic solution containing H_2O_2 which mimicked the tumor microenvironment, the quenching degree of MB significantly increased and the chromogenic degree of TMB rapidly enhanced (Fig. S6 in Supporting information). Specifically, the absorption peak at 644 nm of MB decreased and that at 652 nm of TMB increased dramatically under the conditions of pH 4.0 containing H_2O_2 (Fig. S7 in Supporting information), which demonstrated that LIPN could be dissociated in acidic environments and act as an efficient chemodynamic agent to produce ·OH in cancer cells. Additionally, we detected the peroxidase (POD)-like specific activity of LIPN. As shown in Fig. S8 (Supporting information), the K_m of LIPN was determined to be 2.7 mmol/L. Compared with the kinetic parameters of other nanozymes (Table S1 in Supporting information), LIPN showed lower K_m, indicating its great POD-like catalytic performance. Meanwhile, we also detected the specific activity of LIPN, which was calculated to be 1252.7 U/g.

As shown in Figs. 1e and f, LIPN could be uptaken by 4T1 cells and the internalization increased with the prolonged incubation time characterized by confocal laser scanning microscopy (CLSM) and flow cytometry. To elucidate the amplified oxidative damage by Fenton reaction to tumor cells, 2′,7′-dichlorodihydrofluorescein diacetate (DCFH-DA) and hydroxyphenyl fluorescein (HPF) were used to characterize the ROS and ·OH changes in 4T1 cells after LIPN treatment, respectively. As expected, LIPN-treated 4T1 cells exhibited the strongest ROS and ·OH fluorescence compared with that incubated with β-LP and β-LP diminished nanoparticles (IPN) (Fig. 2a, Fig. S9 in Supporting information). Due to the enhancement of cellular ·OH, LIPN showed greater cytotoxicity than β-LP in 4T1 tumor cells with the half maximal inhibitory concentration (IC_{50}) declined from 0.4 μg/mL to 0.2 μg/mL. Meanwhile, the IC_{50} of LIPN in 293T normal cells was calculated to be 3.1 μg/mL (Figs. 2b and c). The much higher cytotoxicity against 4T1 tumor cells than that against 293T normal cells was because of the overexpressed NQO1 in cancer cells which triggered cascade amplification of the cellular ROS [28]. The results indicated LIPN could act as an efficient chemodynamic agent against tumors with minimal side effect to normal tissue.

Furthermore, typical ICD signals including calreticulin (CRT), high mobility group box 1 (HMGB1), and ATP, caused by LIPN were tested. These DAMPs were proved to facilitate the recruitment, antigen processing, and presentation, which induced significant cytotoxic T cell infiltration [38-40]. As shown in Figs. 2d and e, the LIPN group led to the highest level of CRT translocation, HMGB1 release and ATP secretion, which were about 3.1, 1.3 and 2.8 folds higher than that of the PBS group (Fig. S10 in Supporting information), respectively. The above results were similar to previous findings that LIPN could specifically amplify the cytotoxic effect on tumor cells.

The *in vivo* tumor inhibition of LIPN was characterized by 4T1 subcutaneous tumor model. All animal experiments were carried out under the protocols approved by the Institutional Animal Care and Use Committee (IACUC) of Zhejiang University (approval No. 20379) in accordance with the institutional guidelines. The tumor-bearing mice were treated by (1) LIPN, (2) β-LP solubilized with hydroxypropyl cyclodextrin (SLP), (3) IPN, and (4) PBS, respectively. The rapid growth of tumors in the mice treated with SLP

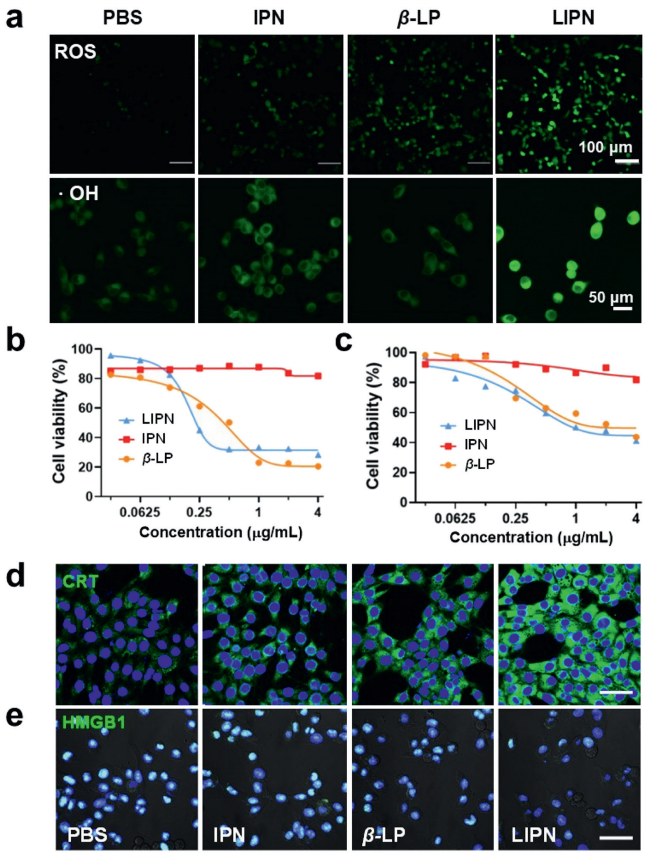

Fig. 2. (a) CSLM images for the cellular ROS and ·OH of 4T1 cells incubated with PBS, IPN, β-LP, and LIPN, respectively. [β-LP] = 0.5 μg/mL. Relative viabilities of (b) 4T1 cells and (c) 293T cells after LIPN and other treatments with equal β-LP concentration for 48 h. CLSM images of (d) CRT and (e) HMGB1 of 4T1 cells with different treatments. Scale bar: 50 μm. Data are presented as mean ± standard deviation (SD) (n = 3).

or IPN implied that the generation of H_2O_2 or ·OH solely by β-LP or iron-polyphenol nanocomplex had limited tumor therapeutic efficiency. However, the group treated with LIPN exhibited the strongest tumor suppression effect with a tumor growth inhibitory rate of 76.5%, which could be ascribed to the cascade ROS amplification and subsequently chemodynamic damage in tumor cells (Figs. 3a–c). Fig. 3d showed steady body weight in PBS, IPN and LIPN groups rather than SLP group during treatment, however, the SLP group recovered its body weight after drug withdrawal, suggesting LIPN greatly reduced the systemic toxicity of β-LP. After 5 rounds of treatments, hematoxylin and eosin (H&E) staining and routine blood test and blood chemistry analysis were conducted to investigate the biosafety and antitumor activity of LIPN (Figs. S11 and S12 in Supporting information). No obvious physiological damages were found in major organs (liver, heart, lung, spleen, and kidney) of the LIPN group, demonstrating LIPN's great biocompatibility. Additionally, the H&E staining of tumor sections showed that LIPN caused severe damage with cell fragmentation in tumor tissue, and those of the other groups almost had no change. The blood circulation time of β-LP in LIPN was determined with $t_{1/2}(\alpha)$ of 0.03 h, and $t_{1/2}(\beta)$ of 5.03 h, respectively (Fig. S13a in Supporting information). LIPN nanocomplex contained Fe^{3+}, which could be used as a magnetic resonance contrast agent for tumor imaging, and the results also showed the effective accumulation in the tumor after 24 h treatment (9.9 μg/g, Figs. S13b and S14 in Supporting information) with good tumor targeting ability. The *in vivo* ICD effect like the expression of CRT and HMGB1 induced by LIPN in

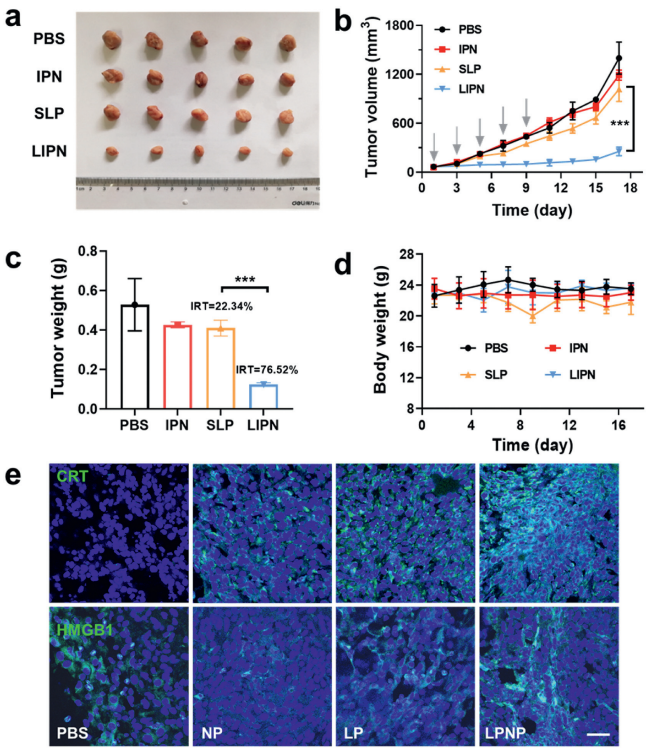

Fig. 3. (a) Tumor photo, (b) tumor progression profiles, (c) tumor weight, and (d) body weight of mice bearing 4T1 subcutaneous tumors with different treatments ($n = 5$). [β-LP] = 5 mg/kg, i.v. with 5 times. (e) Immunofluorescence observation of CRT, HMGB1 in tumor tissues. Scale bar: 200 μm. Data are presented as mean ± SD ($n = 3$). $^{***}P < 0.001$. IRT: tumor growth inhibitory rate.

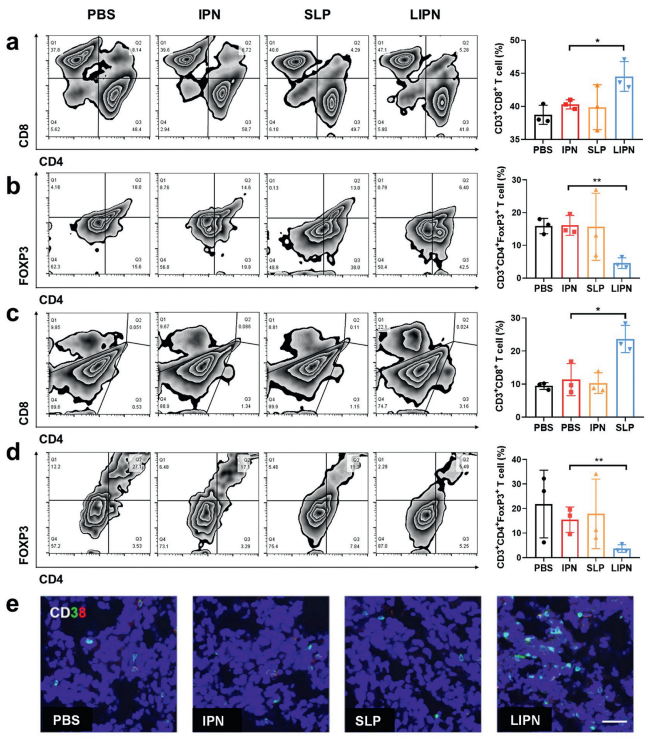

Fig. 4. Flow cytometry analysis of the percentage of $CD3^+$ $CD8^+$ T cells in (a) TDLNs and (c) tumor tissues, as well as $CD3^+$ $CD4^+$ $Foxp3^+$ T cells in (b) TDLNs and (d) tumor tissues. (e) Immunofluorescent staining images of $CD3^+$ and $CD8^+$ T cells in tumor sections after different treatments. Scale bar: 200 μm. Data are presented as mean ± SD ($n = 3$). $^*P < 0.05$, $^{**}P < 0.01$.

the tumor were also tested by immunofluorescent staining. Compared with the control groups, the LIPN group had significant increased CRT and HMGB1 levels, indicated the chemodynamic therapy with LIPN could efficiently induce ICD (Fig. 3e).

The infiltration of cytotoxic T lymphocytes (CTLs) in tumor-draining lymph nodes (TDLNs) and tumors tissues were characterized by proportions of $CD8^+$ cytotoxic T cells and $CD4^+$ $FoxP3^+$ regulatory T cells (Fig. 4). The LIPN group exhibited the highest increase of $CD8^+$ T cells and decrease of $CD4^+$ $FoxP3^+$ T cells in TDLNs and tumor tissues (Figs. 4a–d). Specifically, the percentages of $CD8^+$ T cells in TLDNs and tumor tissues treated by LIPN (44.5%, 23.6%) were higher than that of the PBS group (38.7%, 9.4%). Similarly, the percentage of $CD4^+$ $Foxp3^+$ T cells in TDLNs and tumors treated by LIPN decreased from 15.9% and 4.6% to 21.8% and 3.7%, respectively, demonstrating an alleviate immune suppression in tumors. The immune-fluorescent staining analysis of tumor sections also demonstrated the highest $CD8^+$ T cells recruitment by LIPN treatment (Fig. 4e). Furthermore, the secretion level of interferon (IFN)-γ and tumor necrosis factor (TNF)-α in the serum of the LIPN group were significantly higher than that of the PBS group (Fig. S15 in Supporting information). All these results suggested the enhanced ICD could increase the infiltration of cytotoxic T lymphocytes with decreasing the ratio of regulatory T cells in tumor, and enhance the secretion proinflammatory cytokines, which led to efficient chemodynamic antitumor efficacy of LIPN.

In summary, a pH-responsive LIPN was facilely prepared, which could disassociate in the tumors to release β-LP, Fe^{3+}, and TA. The β-LP selectively elevated H_2O_2 in cancer cells and TA reduced Fe^{3+} to Fe^{2+}, collectively enhancing the chemodynamic toxicity through Fenton reaction between H_2O_2 and Fe^{2+}. LIPN efficiently induced strong ICD reflected by increased translocation of CRT, release of HMGB1 and secretion of ATP. Additionally, LIPN exhibited excellent tumor-targeting capability with the highest accumulation in the tumor. Therefore, LIPN showed efficient antitumor activity with a tumor growth inhibitory rate of 76.5% in 4T1 subcutaneous tumor model. The immune analysis suggested that the treatment with LIPN increased the infiltration of $CD8^+$ cytotoxic T lymphocytes and decreased the proportion of $CD4^+$ $FoxP3^+$ regulatory T lymphocytes in tumor tissues, implying the potential synergism of chemodynamic and immune therapy from LIPN. This work demonstrated a method to enhance ICD of chemodynamic therapy through selective cascade amplification of ROS in cancer cells.

Declaration of competing interest

The authors declare that they have no known competing financial interests or personal relationships that could have appeared to influence the work reported in this paper.

CRediT authorship contribution statement

Xueying Shi: Writing – review & editing, Methodology, Data curation, Conceptualization. **Xiaoxuan Zhou:** Resources, Methodology, Data curation. **Bing Xiao:** Methodology. **Hongxia Xu:** Software. **Wei Zhang:** Project administration. **Hongjie Hu:** Visualization, Funding acquisition. **Shiqun Shao:** Software, Formal analysis. **Zhuxian Zhou:** Supervision. **Youqing Shen:** Visualization, Validation, Methodology. **Xiaodan Xu:** Writing – original draft, Software, Methodology, Formal analysis, Data curation, Conceptualization. **Jianbin Tang:** Writing – review & editing, Visualization, Validation, Resources, Funding acquisition, Formal analysis, Data curation, Conceptualization.

Acknowledgments

This work was financially supported by the National Natural Science Foundation of China (Nos. T2293753, 52203194), the National Key R&D Program of China (No. 2021YFA1201200), the Natural Science Foundation of Zhejiang Province (No. LR18E030002), and 2023 Hangzhou West Lake Pearl Project Leading Innovative Youth Team Project.

Supplementary materials

Supplementary material associated with this article can be found, in the online version, at doi:10.1016/j.cclet.2024.110178.

References

[1] Y. Wang, C. Zhang, S. Han, et al., Chin. Chem. Lett. 35 (2024) 109578.
[2] H. Liu, T. Nie, X. Duan, et al., J. Control. Release 359 (2023) 132–146.
[3] J. Shi, P.W. Kantoff, R. Wooster, O.C. Farokhzad, Nat. Rev. Cancer 17 (2017) 20–37.
[4] L. Xie, G. Wang, W. Sang, J. Li, et al., Biomaterials 269 (2021) 120638.
[5] L. Li, Y. Li, C.H. Yang, et al., Adv. Funct. Mater. 30 (2020) 1908961.
[6] W. Yan, T. Lang, X. Qi, Y. Li, Curr. Opin. Biotech. 66 (2020) 36–43.
[7] C. Xu, Y. Yu, Y. Sun, et al., Adv. Funct. Mater. 29 (2019) 1905213.
[8] Y. Li, Z. Duan, D. Pan, et al., Adv. Mater. 35 (2023) e2210161.
[9] J. Lu, X. Liu, Y.P. Liao, et al., ACS Nano 12 (2018) 11041–11061.
[10] D.Y. Wong, W.W. Ong, W.H. Ang, Angew. Chem. Int. Ed. 54 (2015) 6483–6487.
[11] H.M. Chen, P.H. Wang, S.S. Chen, et al., Cancer Immunol. Immun. 61 (2012) 1989–2002.
[12] L. Luo, Y. Qi, H. Zhong, et al., Acta Pharm. Sin. B 12 (2022) 424–436.
[13] Z. Tang, Y. Liu, M. He, et al., Angew. Chem. Int. Ed. 58 (2019) 946–956.
[14] Y. Dai, Z. Yang, S. Cheng, et al., Adv. Mat. 30 (2018) 1704877.
[15] Z. Dong, L. Feng, Y. Chao, et al., Nano Lett. 19 (2019) 805–815.
[16] J. Hu, S. Liu, J. Control. Release 319 (2020) 333–343.
[17] P. Yu, X. Li, G. Cheng, et al., Chin. Chem. Lett. 32 (2021) 2127–2138.
[18] X. Li, R. Luo, X. Liang, Q. Wu, C. Gong, Chin. Chem. Lett. 33 (2022) 2213–2230.
[19] Z. Tang, Q. He, J. Zhou, et al., Chin. Chem. Lett. 35 (2024) 109742.
[20] Y. Yu, Y. Meng, X. Xu, et al., ACS Nano 17 (2023) 3334–3345.
[21] F. Zhang, F. Li, G.H. Lu, et al., ACS Nano 13 (2019) 5662–5673.
[22] Y. Yang, J. Tang, P.L. Abbaraju, et al., Angew. Chem. Int. Ed. 57 (2018) 11764–11769.
[23] F. Liu, L. Lin, Y. Zhang, et al., Adv. Mater. 31 (2019) 1902885.
[24] F. Jiang, C. Yang, B. Ding, et al., Chin. Chem. Lett. 33 (2022) 2959–2964.
[25] S. Pan, B. Cao, D. Yuan, et al., Chin. Chem. Lett. 35 (2024) 109185.
[26] Y. Zhuang, S. Han, Y. Fang, H. Huang, J. Wu, Coordin. Chem. Rev. 455 (2022) 214360.
[27] K. Ni, T. Aung, S. Li, et al., Chem 5 (2019) 1892–1913.
[28] X. Li, Z. Liu, A. Zhang, et al., Nat. Commun. 10 (2019) 3251.
[29] M. Ye, Y. Han, J. Tang, et al., Adv. Mater. 29 (2017) 1702342.
[30] K. Wang, B. Yang, H. Ye, et al., ACS Appl. Mater. Interfaces 11 (2019) 18914–18922.
[31] T. Luan, L. Cheng, J. Cheng, et al., ACS Appl. Mater. Interfaces 11 (2019) 25654–25663.
[32] L. Dai, X. Li, X. Duan, et al., Adv. Sci. 6 (2019) 1801807.
[33] T. Liu, W. Liu, M. Zhang, et al., ACS Nano 12 (2018) 12181–12192.
[34] C. Xu, Y. Wang, H. Yu, H. Tian, X. Chen, ACS Nano 12 (2018) 8255–8265.
[35] N. Guo, Y. Xia, Y. Duan, et al., Chin. Chem. Lett. 34 (2023) 107542.
[36] X. Hai, Y. Li, K. Yu, et al., Chin. Chem. Lett. 32 (2021) 1215–1219.
[37] L. Liu, L. Yin, H. Bian, N. Zhang, Chin. Chem. Lett. 31 (2020) 501–504.
[38] D.R. Green, T. Ferguson, L. Zitvogel, G. Kroemer, Immunology 9 (2009) 353–363.
[39] C.D. Phung, H.T. Nguyen, J.Y. Choi, et al., J. Control. Release 315 (2019) 126–138.
[40] X. Feng, W. Xu, J. Liu, et al., Sci. Bull. 66 (2021) 362–373.